DOI 10.5162/Ultrasonic2025/B15-a2

Ultrasound Transducer Array with Imaging and Power Output Capabilities for Tumor Perfusion Enhancement

Teng Zhang[1], Lijun Xu[1], and Jianguo Ma[1]
[1]School of Instrumentation and Optoelectronics Engineering, Beihang University, Beijing, China
majianguo@buaa.edu.cn

Abstract: Ultrasound-mediated tumor perfusion enhancement offers a promising strategy to overcome treatment resistance. To enable precise therapy, we developed a dual anti-matching layer transducer array capable of simultaneous imaging and power output. Simulation results show a 31% increase in pulse-echo sensitivity and a reduction in –6 dB bandwidth from 61.9% to 55.5%. The fabricated transducer array achieves a –6 dB bandwidth of 56.5%, close to the simulation, with uniform acoustic output suitable for therapeutic use.

Keywords: Dual anti-matching layers, imaging-guided therapy, transducer design, ultrasound-mediated tumor perfusion enhancement, ultrasound transducer array.

Introduction

Chemotherapy and radiotherapy are currently the main clinical approaches for treating most malignant tumors, while immunotherapy, as an emerging modality, shows promising potential for future development. However, all of these treatment methods often face therapeutic resistance in hypoperfused tumors, which leads to suboptimal efficacy and increased risk of recurrence [1].

In recent years, ultrasound-mediated tumor perfusion enhancement has provided a novel strategy to address this challenge [2, 3]. This technique involves the injection of microbubbles into the bloodstream, followed by ultrasonic stimulation targeted at the tumor region to enhance local perfusion, thereby improving drug delivery and overcoming resistance in hypoperfused tumors [4].

In this approach, the ultrasound transducer must not only deliver sufficient acoustic power to effectively stimulate tissue but also provide real-time imaging capability to ensure treatment precision and safety [5]. If separate transducers are used for imaging and therapy, accurate localization of the therapeutic focus within the image becomes difficult. In contrast, using a single transducer for both functions ensures that the imaging and therapeutic beams share the same path, allowing for direct visualization of the treatment focus in the image and thereby improving targeting accuracy. Therefore, the development of an ultrasound transducer with both imaging and power output capabilities is essential for ultrasound-mediated tumor perfusion enhancement therapy.

However, traditional ultrasound transducers face challenges in meeting this dual-functional requirement. Imaging transducers typically employ a high-acoustic-impedance backing layer behind the piezoelectric element to absorb backward waves and improve axial resolution [6]. However, this design results in 20–30% of the total acoustic energy being converted into heat within the backing layer, reducing transmission efficiency and potentially causing thermal deformation of the backing material, which may damage the transducer. In contrast, therapeutic transducers typically employ an air backing layer with extremely low acoustic impedance to avoid this issue, making them suitable for applications requiring high acoustic power [7], such as high-intensity focused ultrasound (HIFU). However, the air backing layer does not provide mechanical support, and since the piezoelectric array in imaging transducer arrays is relatively fragile, an air backing layer is not suitable for imaging transducers.

To address these challenges, this study developed an ultrasound transducer array incorporating a dual anti-matching layers (AML) structure. By stacking multiple layers of materials to form an equivalent low-impedance backing, this structure provides high acoustic reflectivity and sufficient mechanical support. On one hand, it improves the forward transmission efficiency of the emitted acoustic energy; on the other, it preserves imaging resolution. As such, it enables simultaneous high-performance imaging and high-power delivery, meeting the performance requirements of ultrasound-mediated tumor perfusion enhancement.

Transmission Line Model and Dual Anti-Matching Structure

Traditional ultrasound transducers typically consist of a matching layer, a piezoelectric layer, and a backing layer arranged from front to rear. When electrically excited, the piezoelectric layer emits acoustic waves both forward (toward the matching layer) and back-

DOI 10.5162/Ultrasonic2025/B15-a2

ward (toward the backing layer). To improve reflection of the backward waves, this study introduces two intermediate layers between the piezoelectric layer and the backing layer, referred to as the 1st AM layer and 2nd AM layer (see Fig. 1).

Due to the similarity between the propagation characteristics of acoustic waves in media and electromagnetic waves in transmission lines, microwave transmission line theory is adopted to analyze the energy transfer efficiency of the multi-layer structure [8]. Since the piezoelectric layer is acoustically impedance-matched to the front load via the matching layers, it can be regarded as a pure resistor with an impedance of Z_p in the transmission line model. The backing layer, due to its thickness being much greater than the wavelength, is also treated as a pure resistance Z_b. When the thicknesses of the 1st AM layer and the 2nd AM layer are much smaller than their respective acoustic wavelengths, they can be modeled as transmission line segments with characteristic impedances Z_1 and Z_2, respectively (see Fig. 1).

According to transmission line theory, the acoustic energy transmission efficiency can be calculated as

$$T_I = 1 - |R_p|^2, \tag{1}$$

where R_p is the acoustic pressure reflection coefficient, which can be calculated as

$$R_p = \frac{Z_2 - Z_p^*}{Z_2 + Z_p}, \tag{2}$$

where Z_p^* is the complex conjugate of the impedance Z_p. Z_2 is the equivalent impedance of the dual AML, which is calculated as

$$Z_2 = Z_{a1} \cdot \frac{Z_1 + jZ_{a1}\tan(k_{a1}l_{a1})}{Z_{a1} + jZ_1\tan(k_{a1}l_{a1})}, \tag{3}$$

$$Z_1 = Z_{a2} \cdot \frac{Z_b + jZ_{a2}\tan(k_{a2}l_{a2})}{Z_{a2} + jZ_b\tan(k_{a2}l_{a2})}, \tag{4}$$

As indicated by equations Eq. (1)–(4), when $Z_{a1} < Z_p$, $Z_{a2} > Z_{a1}$, and $Z_b < Z_{a2}$, the structure exhibits high acoustic reflectivity.

In this study, the 1st AM layer is made of epoxy resin (2.7 MRayl), the 2nd AM layer is made of tungsten steel (97.2 MRayl), and the backing layer is made of a mixture of alumina and epoxy resin (5.0 MRayl). The transmission efficiency distribution of the dual AML structure can be calculated based on transmission line theory. Without the dual AML structure, approximately 45% of the backward acoustic energy transmits into the backing layer, with an insertion loss of around –3.5 dB. The dual AML structure exhibits a wideband suppression region, where the strongest suppression occurs when both AML

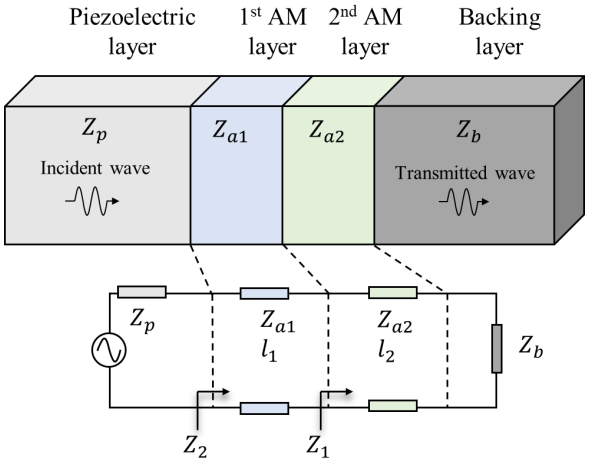

Fig. 1: Schematic view of the equivalent circuits for the dual AML structure.

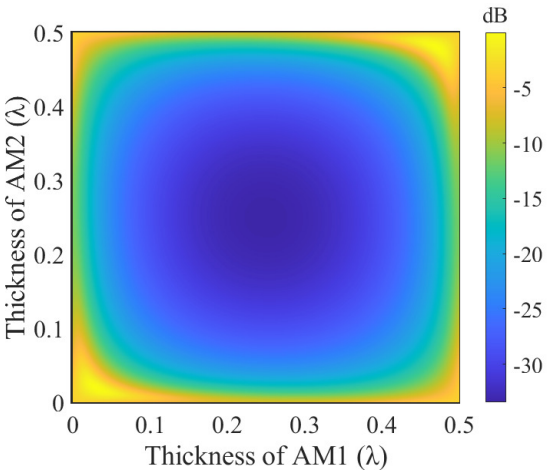

Fig. 2: Insertion loss of double AML structure.

layers are a quarter-wavelength thick. Under this configuration, the insertion loss reaches approximately –33.0 dB, corresponding to a transmission efficiency of only 0.05% (see Fig. 2). This indicates that nearly all the backward-propagating energy is reflected back into the load rather than entering the backing layer, thereby significantly reducing thermal loss and enhancing forward transmission efficiency.

In addition to acoustic performance, the AML structure also provides robust mechanical support, making it suitable for ultrasound transducers that require both high power output and reliable imaging performance.

Transducer Design and Fabrication

In this study, we designed and fabricated an ultrasound transducer array with the dual AML. The transducer consists of 128 elements, with a total array length of approximately 65 mm and a width of 13 mm.

DOI 10.5162/Ultrasonic2025/B15-a2

The design center frequency is 2.8 MHz. The pitch between elements is 0.508 mm, and the kerf width is 0.04 mm.

The backside of the piezoelectric layer is equipped with the dual AML structure (see Fig. 3). The 1st AM layer is composed of epoxy resin, while the 2nd AM layer is made of tungsten steel. Both AM layers have a thickness of one-quarter wavelength at the center frequency to effectively reflect the backward-propagating acoustic waves. Behind the 2nd AM layer, a 10 mm-thick composite backing layer made of alumina and epoxy provides mechanical support.

Although the dual AML structure effectively enhances power output by reflecting backward waves, it also tends to increase pulse duration and reduce bandwidth. For traditional backing layer designs, the primary function is to absorb backward acoustic waves and shorten the pulse duration. The AML structure, equivalent to an extremely low-impedance backing, essentially loses the ability to absorb backward waves, resulting in significantly prolonged pulses. Therefore, precise design of the matching layers is essential to ensure reasonable pulse length and bandwidth for imaging. In this work, a double matching layers structure is employed at the front of the transducer to effectively shorten pulse duration and broaden bandwidth.The detailed structural parameters of each layer are listed in Tab. 1.

The Krimholtz–Leedom–Matthaei (KLM) model was used to simulate the pulse-echo response of the proposed transducer and compare it with that of a traditional backing layer structure. The pulse-echo signals were post-processed by envelope detection. Simulation results show that the proposed transducer achieves a pulse-echo sensitivity of 6.24 mV/V, compared to 4.77 mV/V for the traditional design—an increase of approximately 31%, indicating a significantly stronger output (see Fig. 4). The –6 dB bandwidths of the proposed and traditional transducers are 55.5% and 61.9%, respectively, reflecting a decrease of about 6.4%. These results demonstrate that the proposed design can significantly enhance power output while maintaining comparable imaging performance.

The fabrication process of the proposed transducer is as follows: A PZT-5H piezoelectric ceramic was selected as the base. The dual AML were bonded sequentially to the bottom surface of the piezoelectric ceramic, following the designed thickness. A prefabricated double matching layer was bonded to the top surface. The piezoelectric ceramic was then diced into 128 elements, and the kerfs were filled with epoxy resin. The top electrode of the piezoelectric ceramic was grounded, while signal wires were soldered to the bottom electrodes of each element. Finally, the backing layer was attached behind the 2nd AM layer,

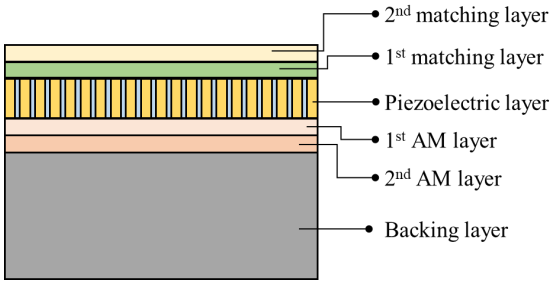

Fig. 3: Structural diagram of the dual AML transducer array.

Tab. 1: Transducer parameters

Structure	Velocity (m/s)	Density (kg/m^3)	Thickness (μm)
2nd matching	2600	1040	214
1st matching	1554	6253	133
Piezoelectric	4400	7500	720
1st AM	2600	1040	232
2nd AM	7200	13500	643
Backing	2307	2180	10000

and the transducer was encapsulated to complete the fabrication.

Transducer Performance

The acoustic performance of the fabricated dual AML transducer array was experimentally evaluated. A pulse-echo test was conducted using an ultrasound pulser/receiver (5073PR, Olympus Corp., USA), which generated excitation pulses with an energy of 8 μJ. The echo signals were captured and recorded using an oscilloscope (MSO54, Tektronix Inc., USA). A reflecting surface was placed in front of the transducer to ensure wave reflection.

The measured pulse-echo peak amplitude was

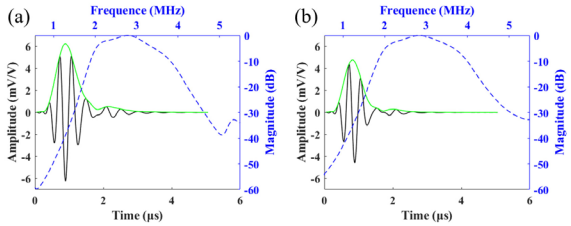

Fig. 4: Pulse-echo waveforms and spectra from KLM simulations of (a) AML and (b) traditional transducers.

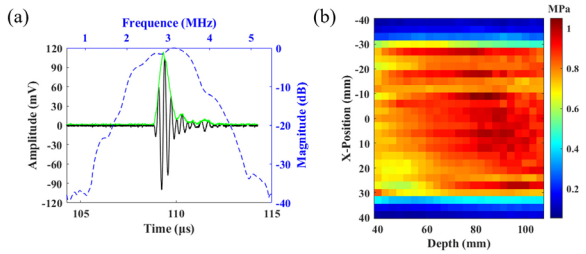

Fig. 5: Measured (a) pulse-echo waveforms and spectra, and (b) acoustic field distribution of the AML transducer array

127.8 mV, and the –6 dB bandwidth was 56.5% (see Fig. 5). The measured bandwidth was slightly higher than the simulation result, which may be attributed to the one-dimensional nature of the KLM model, whereas the actual transducer is a three-dimensional structure—potentially affecting the accuracy of bandwidth prediction.

In addition, the acoustic field of the transducer was scanned using a hydrophone (NH0200, Precision Acoustics Ltd., UK), which was precisely positioned by a three-axis motorized stage. A custom-developed 128-channel ultrasonic driving system was used to excite the transducer with a 2.8 MHz, 5-cycle square wave signal at 20 V. The hydrophone signals were acquired and digitized using an oscilloscope (MSO54, Tektronix Inc., USA).

Experimental results indicate that the transducer maintains good pressure uniformity within a depth range of 40–110 mm, with a lateral –6 dB beamwidth of approximately 60 mm (see Fig. 5). The peak negative pressure in this region exceeds 0.5 MPa, corresponding to a mechanical index (MI) of 0.3, which meets the typical threshold for ultrasound-mediated tumor perfusion enhancement (MI $\approx$ 0.3) [2].

Conclusion

In summary, we developed an ultrasound transducer array with a dual AML structure that enables the integration of imaging and acoustic power output. The proposed design effectively enhances acoustic power transmission through improved reflection of backward waves, while maintaining imaging performance. Both simulation and experimental evaluations demonstrated the transducer's suitability for ultrasound-mediated tumor perfusion enhancement. Overall, this transducer design offers a promising approach for integrating therapeutic ultrasound with real-time imaging, enabling more precise and efficient tumor perfusion enhancement.

Acknowledgment

This research was funded by the Fundamental Research Funds for the Central Universities (JKF-20240571).

References

[1] K. Graham and E. Unger. "Overcoming tumor hypoxia as a barrier to radiotherapy, chemotherapy and immunotherapy in cancer treatment". In: *International Journal of Nanomedicine* 13 (2018), pp. 6049–6058. DOI: 10.2147/IJN.S140462.

[2] Y. Zhang et al. "Effect of diagnostic ultrasound and microbubble-enhanced chemotherapy on metastasis of rabbit VX2 tumor". In: *Medical Physics* 48 (2021), pp. 3927–3935. DOI: 10.1002/mp.14867.

[3] N. Tang et al. "Sononeoperfusion: a new therapeutic effect to enhance tumour blood perfusion using diagnostic ultrasound and microbubbles". In: *Cancer Imaging* 23 (2023), p. 29. DOI: 10.1186/s40644-023-00545-y.

[4] N. Li et al. "Tumor perfusion enhancement by ultrasound stimulated microbubbles potentiates PD-L1 blockade of MC38 colon cancer in mice". In: *Cancer letters* 498 (2021), pp. 121–129. DOI: 10.1016/j.canlet.2020.10.046.

[5] Y. Cai et al. "Ultrasound transducers with both imaging and power output capabilities by anti-matching at backing layers". In: *Applied Physics Letters* 124 (2024), p. 072201. DOI: 10.1063/5.0191191.

[6] Y. Cai et al. "Axial super-resolution ultrasound imaging with quasi-monopolar pulses from a dual-frequency transducer". In: *IEEE Transactions on Instrumentation and Measurement* 72 (2023), p. 9500710. DOI: 10.1109/TIM.2023.3234032.

[7] J. K. Woodacre, T. G. Landry, and J. A. Brown. "Fabrication and characterization of a 5 mm x 5 mm aluminum lens-based histotripsy transducer". In: *IEEE Transactions on Ultrasonics, Ferroelectrics, and Frequency Control* 69 (2022), pp. 1442–1451. DOI: 10.1109/TUFFC.2022.3152174.

[8] M. Huang et al. "Single- and dual-band RF rectifiers with extended input power range using automatic impedance transforming". In: *IEEE Transactions on Microwave Theory and Techniques* 67 (2019), pp. 1974–1984. DOI: 10.1109/TMTT.2019.2901443.